Draft version November 9, 2022
Typeset using LaTeX **twocolumn** style in AASTeX63

Isotopic Abundance Ratios of C and O in the Dark Cloud L1521E

Jay Motka,[1] Jacob Magnusson,[1] Maya Mancini,[1] and Akash Satpathy[1]

[1] *Department of Astronomy and Steward Observatory, University of Arizona, Tucson, AZ 85721, USA*

ABSTRACT

Isotopic ratios of various molecules from molecular clouds gives us valuable information on the chemical and physical processes that governs the astronomical processes such as star formation. We measure the isotopic abundance ratios of carbon and oxygen in a young starless cloud L1521E using the line emissions of $J = 2-1$ rotational transition in CO and its isotopes. We use CHAOS, a powerful python package to perform data reduction and data analysis on the observed spectra of isotopes of CO in L1521E using SMT at Mt. Graham. The measured ratios, $\frac{^{12}C}{^{13}C}$, $\frac{^{16}O}{^{17}O}$, and $\frac{^{16}O}{^{18}O}$, are 39.95 ± 7.89, 176.57 ± 92.57, and 71.81 ± 14.22, respectively. More precise measurements could be found by using better observational data and improved calculations of line profiles.

Keywords: isotopic ratios, starless core, abundance

1. INTRODUCTION

Different isotopic ratios inside molecular clouds gives us an insight towards the galactic chemical structure and evolution. Furthermore, the elements such as carbon and oxygen are created during stellar nucleosynthesis. As such the isotope abundance ratios of these elements provide valuable information about the physics and chemistry of star formation (Langer & Penzias 1993).

For this purposes carbon-based molecules such as carbon monoxide and its isotopic species are very useful. The spectra of CO and its isotopic species, ^{12}C^{17}O, ^{12}C^{18}O, ^{13}C^{16}O, ^{13}C^{17}O and ^{13}C^{18}O are easier to get on a single object as the frequencies of their $J = 2 - 1$ transitions are not so far apart. Thus, it is possible to simultaneously measure two lines at a time as stated in Section 2.

The chemical compounds of starless and gravitationally bound pre-stellar cores, sometimes also known as dark clouds or dark cores, is substantially informational in understanding the initial physical conditions and chemical structures of the star formation. As such, we present to look at the isotopic abundance ratios of

Corresponding author: Jay Motka
jaymotka@arizona.edu

Table 1. Information of scans and total integration time for each line. The first section is the information from the observation on March 06, 2021. The last two lines are for the new observation on March 07, 2021. These new observations with no contamination were used in our calculations.

Line ($J = 2 - 1$)	Rest Frequency (GHz)	No. of Scans	Total Integration Time (Seconds)
$^{12}C^{16}O$	230.53800000	18	6480
$^{13}C^{16}O$	220.39861950	18	6480
$^{12}C^{17}O$	224.71418700	24	8640
$^{13}C^{17}O$	214.57387300	24	8640
$^{12}C^{18}O$	219.56035410	24	8640
$^{13}C^{18}O$	209.41909830	24	8640
$^{12}C^{16}O$	230.53800000	4	1440
$^{13}C^{16}O$	220.39861950	2	1440

CO and its isotopologues in a starless core situated in Taurus, Lynds 1521E (L1521E).

2. OBSERVATIONS AND DATA ANALYSIS

We used the Submillimeter Telescope (SMT) at Mt. Graham with 10 meter diameter for this observation. The front end used was 1.3 mm receiver, that can observe ALMA Band 6 (205-280 GHz). The back end used was 4 IF mode with 32 MHz bandwidth and 250 KHz resolution. These equipments were the most suitable as the $J = 2-1$ transition frequencies of the isotopologues of CO varies in between 209 GHz to 231 GHz as shown in the Table 1.

Given the combination of mixer and amplifier, the sky frequency (ν_{sky}) is determined through a chosen local oscillator frequency (ν_{LO}) and intermediate frequency (ν_{IF}), according to the formula,

$$\nu_{sky} = \nu_{LO} \pm \nu_{IF}. \tag{1}$$

At SMT, the intermediate frequency range is ν_{IF} = 4-8 GHz. Thus, Equation 1 implies that we can observe 4-8 GHz above and below the chosen LO frequency. As such, we chose three different LO frequency such that we could observe then pairs of $^{12}C^{16}O$ and $^{13}C^{16}O$ lines, $^{12}C^{17}O$ and $^{13}C^{17}O$ lines, $^{12}C^{18}O$ and $^{13}C^{18}O$ lines, simultaneously.

The observing mode used was beam switching with the beam throw of ± 2 arcmins and switching rate of 2.5 Hz. In the beam switching mode, the equipment switches between the source and background within the given beam throw at the given switching rate. In doing so, the background noise is subtracted from the source intensity at each switching cycle.

Given an expected line amplitude (T_A), the signal to noise ratio is T_A/σ_T. Here, σ_T is defined as,

$$\sigma_T = \sqrt{\frac{2}{\tau\Delta\nu}} T_{sys}, \tag{2}$$

where T_{sys} is system temperature, $\Delta\nu$ is bandwidth, and τ is the integration time. 1.3 mm receiver at SMT has about typical system temperature of 200-275 K at about 230GHz. Using Equation 2, we calculated inte-

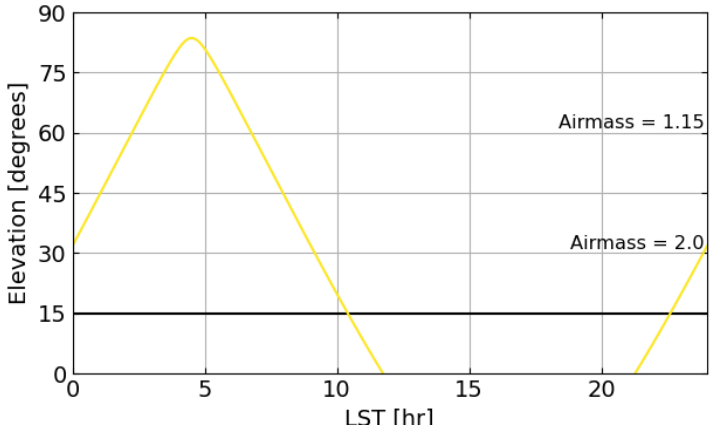

Figure 1. Elevation of L1521E as a function of LST.

gration time of 90 s per sample, given 4 samples per scan, to get approximate good signal-to-noise ratios for each line.

L1521E has the J2000.0 coordinates (RA, Dec) of (04:29:21.0, 26:14:19.0) and the velocity of about 6.8 LSR (Local Standard of Rest). Given this coordinates, we used some programming to determine the best possible time to start the observation. See the elevation of L1521E as a function of LST in Figure 1. The observation was done from 3 LST to 9 LST on March 06, 2021.

Calibration is usually done by looking at a bright continuum source to get the right pointing. As such, we started the observation by calibrating with respect to Mars and then started the observation of the $J = 2 - 1$ transition lines of CO and its isotopic species in L1521E. The total integration time for each line is given in Table 1.

During the observation of $^{12}C^{16}O$ and $^{13}C^{16}O$ lines, we observed an absorption line right next to the emission line in each scan of $^{12}C^{16}O$ line emission. As such, we were not able to take the correct scans of these lines. Upon further investigation, we arrived at the conclusion that this error occurred since we were not able to find an off-position during the beam switching where we could point the telescope towards that had no emission in $^{12}C^{16}O$ line. Thus, while subtracting the noise at off-position from the line emission at the source, we also subtracted the line emission coming from the off-position, which resulted into the contamination. Following the same observing procedure, we were able to take some new scans of $^{12}C^{16}O$ and $^{13}C^{16}O$ line emissions without any contamination on March 07, 2021 at about 1 LST given a new off-position. The information containing these new scans is shown in Table 1. We used these new scans of with no contamination for our calculations regarding $^{12}C^{16}O$ and $^{13}C^{16}O$ lines.

To perform data reduction and analyse the data we utilized a python package called CHAOS (Computations for Heterodyne Analysis, Observations, and Science), which is designed as a python-based alternative to legacy single-dish data reduction software such as CLASS. CHAOS is designed to allow easy python scripting of customizable data reduction pipelines.

We first converted the x-axis of spectra from frequency units to velocity units using the Doppler effect according to,

$$v = c\,\frac{\nu_0 - \nu}{\nu_0},$$

where ν_0 is the rest frequency, ν is the observed frequency due to Doppler effect for motion at velocity v. Then, we set up masks on the scans of each line according to the respective velocity range shown in Table 2.

Table 2. Integrated temperatures and signal to noise ratios given the velocity range of integration and masks for each line emission from L1521E.

Line ($J = 2-1$)	Δv (Km/s)	$\int_{\Delta v} T_R\,dv$ K km/s	SNR
$^{12}C^{16}O$	-2.5 to 1.5	6.0332 ±0.0346	174.365
$^{13}C^{16}O$	-1.4 to 1.4	2.0895 ±0.0288	072.478
$^{12}C^{17}O$	-2.2 to 1.5	0.3632 ±0.0071	051.277
$^{13}C^{17}O$	-2.0 to 1.5	0.0148 ±0.0078	001.908
$^{12}C^{18}O$	-1.0 to 0.7	0.7058 ±0.0045	158.150
$^{13}C^{18}O$	-1.5 to 1.5	0.0312 ±0.0062	005.063

After setting the masks over the specific velocity range as not to lose any data on the line emission, we removed the noise from the rest of the spectra using the baseline fit of polynomial of the degree of 5. After the data reduction is completed for each scan of specific lines, they are combined according to the weights of the system temperature during each scan. The scans are weighted according to their system temperature, as the noise is proportional to the system temperature as stated in Equation 2. These combined spectra of each lines along with velocity masks are shown in Figure 2.

Finally, we calculate the integration of temperature over the velocity range shown in Table 2 along with the signal to noise ratio. The results of this analysis are shown in Table 2.

3. THEORY

As stated in Mangum & Shirley (2015), we first write the radiative transfer equation in a form which involves the observable source radiation remperature T_R derived from a differencing measurement,

$$T_R = (J_\nu(T_{ex}) - J_\nu(T_{cmb}))(1 - e^{-\tau_\nu}). \tag{3}$$

Here, $J_v(T)$ is Rayleigh-Jeans equivalent temperature, which is the equivalent temperature of a black body at temperature T. T_{ex} is extinction temperature, T_{CMB} is CMB background temperature, and τ_v is optical depth.

Let us assume optical depth is small for all molecules. However, this assumption is not very valid for $^{12}C^{16}O$. As such, to calculate the isotopic abundance ratio, using $^{12}C^{16}O$ line will not be very useful in our analysis according to this calculation. Thus, using Equation 3, for two different lines, the integrated temperature ratio is:

$$\frac{\int T_{R,1}\,dv_1}{\int T_{R,2\,dv2}} = \frac{\int (J_1(T_{ex}) - J_1(T_{cmb}))\tau_1 dv_1}{\int (J_2(T_{ex}) - J_2(T_{cmb}))\tau_2 dv_2}.$$

If we assume the temperature difference doesn't vary much over our spectral range, then we can eliminate that term from the numerator and denominator. This leaves us with,

$$\frac{\int T_{R,1} dv_1}{\int T_{R,2} dv_2} = \frac{\tau_1 \Delta v_1}{\tau_2 \Delta v_2}.$$

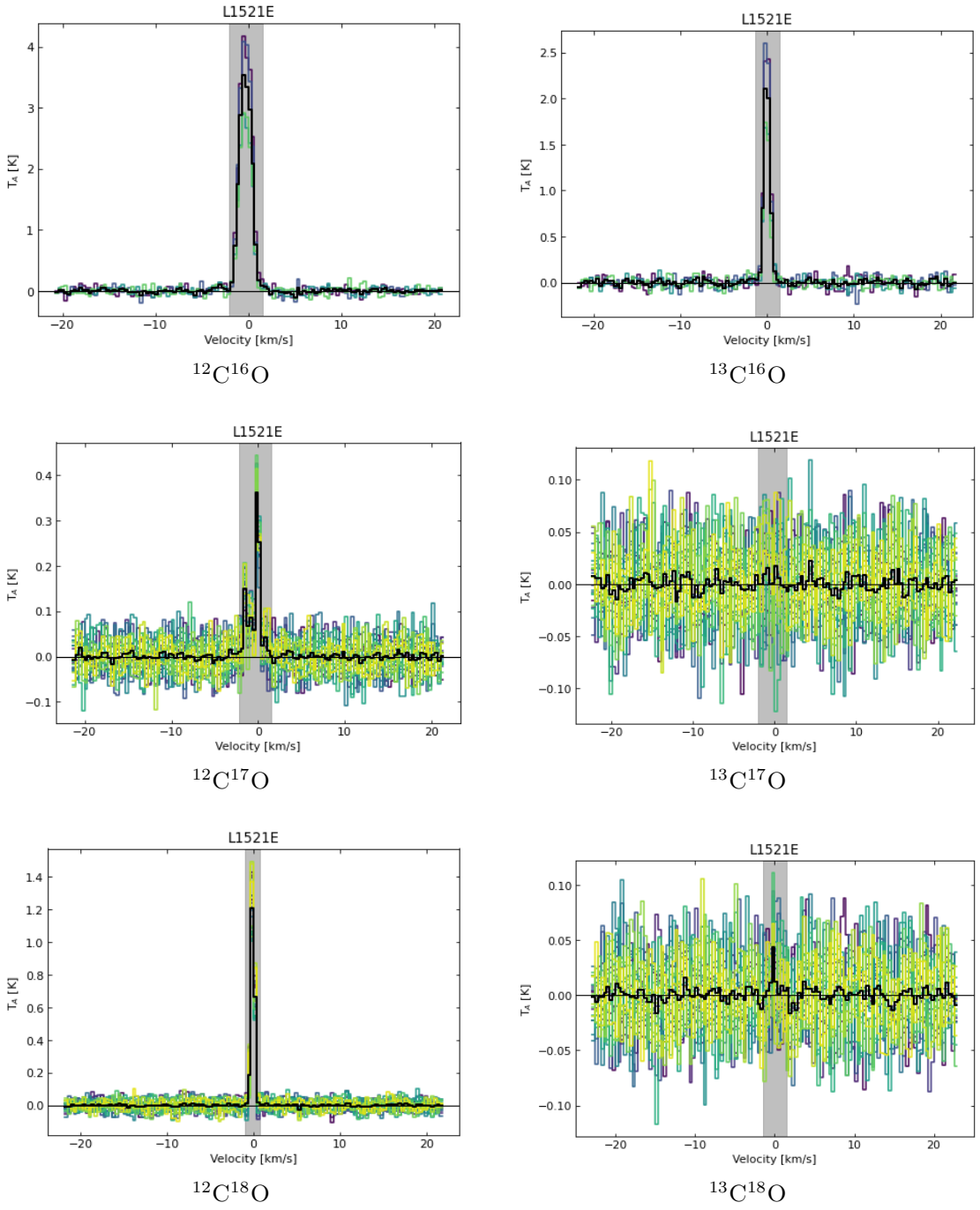

Figure 2. Spectra of the CO (2-1) rotational transition for the isotopologues in L1521E along with velocity masks over the stated velocity range in Table 2.

If we take the optical depth to be some cross section times the column density, then

$$\frac{\tau_1}{\tau_2} = \frac{N_1\sigma_1}{N_2\sigma_2}.$$

Because the frequency difference between these emission lines are small, we can approximate the cross section for each molecule at their respective wavelength for the $J = 2 - 1$ transition to be equal, eliminating the cross sections.

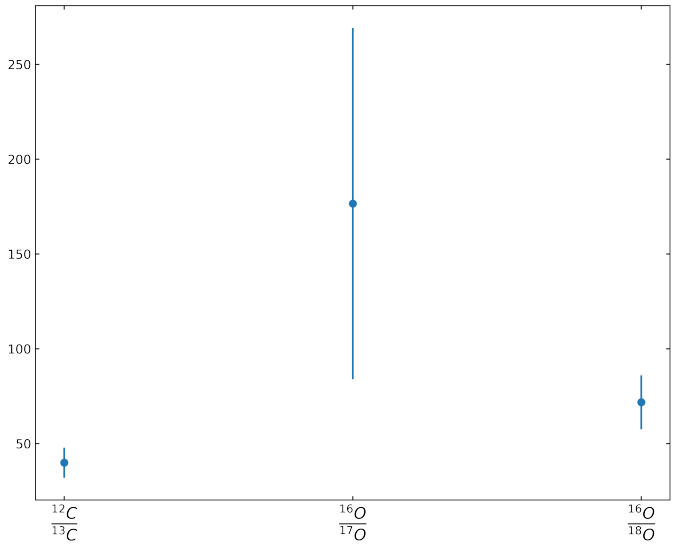

Figure 3. Isotopic abundance ratio in L1521E.

This leads to

$$\frac{\int T_{R,1} dv_1}{\int T_{R,2} dv_2} = \frac{N_1 \Delta v_1}{N_2 \Delta v_2} \tag{4}$$

We now have a direct relation between the ratio of integrated brightness temperature to a ratio of column densities. Lastly, we assume that there is no chemical fractionation (Mangum & Shirley 2015). Thus, the ratio of column density is equal to the abundance ratio of two isotopes.

4. RESULTS

According to the derived Equation 4, we calculated the isotopic ratios of C and O from different line emission using their integrated temperature values and their velocity range as stated in Table 2. Now, as stated in Section 3, due to our assumption of the lines having small optical depths, we ignore $^{12}C^{16}O$ line emission.

Now to calculate isotopic ratios of one element we keep keep the second element of the same species. We calculated the error using the propagation of error given the line ratios, integrated temperatures, and respective errors on integrated temperatures. Finally, we will take the final result to be the one with the least error. The results for these isotopic ratios are shown Table 3 and Figure 3.

Table 3. Calculated line ratios with uncertainties and final results of isotope abundance ratio in L1521E. The final abundance ratio is taken as the one with the least error.

Lines	Line Ratios	$\frac{^{12}C}{^{13}O}$	$\frac{^{16}O}{^{17}O}$	$\frac{^{16}O}{^{18}O}$
$^{12}C^{17}O/^{13}C^{17}O$	023.23 ±12.18			
$^{12}C^{18}O/^{13}C^{18}O$	039.95 ±07.89	39.95	176.57	71.81
$^{13}C^{16}O/^{13}C^{17}O$	176.57 ±92.57	±7.89	±92.57	±14.22
$^{13}C^{16}O/^{13}C^{17}O$	071.81 ±14.22			

5. SCIENTIFIC ANALYSIS AND DISCUSSION

Our calculated isotopic abundance ratios are around the known abundance ratios found for different starless clouds in the local interstellar medium (Langer & Penzias 1993). Our measured value of $\frac{^{12}C}{^{13}C}$ is lower than the observed value of 58.8±3.7 stated in Ikeda et al. (2002).

This might be the case of our poor signal to noise ratio of $^{13}C^{18}O$ line emission along with the assumptions and approximations taken in Section 3. The very large error in the observation of $\frac{^{16}O}{^{17}O}$ is due to very poor signal to noise ratio of $^{13}C^{17}O$ line emission.

The approximation taken in Section 3, namely that the line profile is rectangular can be further modified to fit a Gaussian velocity profile. Langer & Penzias (1993) shows the method of a weighted integrals, which would require a more precise line profile information. Thus, our future ambition is to estimate the most precise line profile for different lines.

6. CONCLUSION

We derived the isotopic abundance ratios, $\frac{^{12}C}{^{13}C}$, $\frac{^{16}O}{^{17}O}$, and $\frac{^{16}O}{^{18}O}$, in a starless cloud Lynds 1521E (L2521E), to be 39.95 ± 7.89, 176.57 ± 92.57, and 71.81 ± 14.22, respectively. These ratios can be made further precise by using a better data as to get the higher SNR for individual line emission. Furthermore, more precise calculation and information regarding properties such as line profiles would increase the precision of these ratios.

7. ACKNOWLEDGEMENT

We thank Dr. Daniel P. Marrone, who supervised this project and guided us through the details of radio observations.

REFERENCES

Ikeda, M., Hirota, T., & Yamamoto, S. 2002, ApJ, 575, 250, doi: 10.1086/341287

Langer, W. D., & Penzias, A. A. 1993, ApJ, 408, 539, doi: 10.1086/172611

Mangum, J. G., & Shirley, Y. L. 2015, PASP, 127, 266, doi: 10.1086/680323